

ReFocus: Reinforcing Mid-Frequency and Key-Frequency Modeling for Multivariate Time Series Forecasting

Guoqi Yu¹ Yaoming Li² Juncheng Wang¹ Xiaoyu Guo² Angelica I. Aviles-Rivero³ Tong Yang²
Shujun Wang¹

Abstract

Recent advancements have progressively incorporated frequency-based techniques into deep learning models, leading to notable improvements in accuracy and efficiency for time series analysis tasks. However, the **Mid-Frequency Spectrum Gap** in the real-world time series, where the energy is concentrated at the low-frequency region while the middle-frequency band is negligible, hinders the ability of existing deep learning models to extract the crucial frequency information. Additionally, the shared **Key-Frequency** in multivariate time series, where different time series share indistinguishable frequency patterns, is rarely exploited by existing literature. This work introduces a novel module, Adaptive Mid-Frequency Energy Optimizer, based on convolution and residual learning, to emphasize the significance of mid-frequency bands. We also propose an Energy-based Key-Frequency Picking Block to capture shared Key-Frequency, which achieves superior inter-series modeling performance with fewer parameters. A novel Key-Frequency Enhanced Training strategy is employed to further enhance Key-Frequency modeling, where spectral information from other channels is randomly introduced into each channel. Our approach advanced multivariate time series forecasting on the challenging Traffic, ECL, and Solar benchmarks, reducing MSE by 4%, 6%, and 5% compared to the previous SOTA iTransformer. Code is available at this **GitHub Repository**: <https://github.com/Levi-Ackman/ReFocus>.

1. Introduction

Accurate forecasting of time series offers reference for decision-making across various domains (Lim & Zohren, 2021; Torres et al., 2021), including weather (Du et al., 2023), economics (Oreshkin et al., 2020), and energy (Dong et al., 2023; Liu et al., 2022b). Especially, long-term multivariate time series forecasting (LMTSF) emerges as a prominent area of interest in academic research (Wang et al., 2024c; Wen et al., 2022) and industrial applications (Cirstea et al., 2022), offering the advantage of capturing complex interdependencies and trends across multiple variables.

Recently, the powerful representation capabilities of neural networks, such as Multi-Layer perception (MLPs) (Yi et al., 2023c; Han et al., 2024), Transformers (Zhou et al., 2022c; Nie et al., 2023), and Temporal Convolution Network (TCNs) (Eldele et al., 2024; Liu et al., 2022a), have significantly advanced deep learning-based LMTSF. These approaches can be broadly categorized into two/three folds: time-domain-based (Han et al., 2024; Nie et al., 2023; Liu et al., 2022a) and frequency-domain-based (Yi et al., 2023c; Zhou et al., 2022c; Eldele et al., 2024) methods, or mixed time & frequency. Time-domain methods are intuitive, handling nonlinearity and non-periodic signals directly from the raw sequence (Li et al., 2023) using Transformers (Zhou et al., 2022a), TCN (Donghao & Xue, 2024), or MLP (Wang et al., 2024a). The latest study (Yi et al., 2024) highlights that time-domain forecasters face challenges such as vulnerability to high-frequency noise, and computational inefficiencies. While frequency-domain-based methods usually transform the time-domain data to the frequency spectrum by Fast Fourier transform (FFT) (Yi et al., 2023a). Then other operations (Self-attention (Zhou et al., 2022c), Linear mapping (Xu et al., 2024a; Yi et al., 2023c), etc.) are employed to extract frequency information. These methods benefit from advantages such as computational efficiency (Fan et al., 2024; Xu et al., 2024a), periodic patterns extracting (Wu et al., 2023; Dai et al., 2024), and energy compaction (Yi et al., 2023c;b).

However, existing frequency-domain-based forecasters usually face TWO significant challenges when dealing with real-world long-term time series: the **Mid-Frequency Spec**

¹Department of Biomedical Engineering, The Hong Kong Polytechnic University, Hong Kong SAR, China ²Data Structures Laboratory, School of Computer Science, Peking University, Beijing, China. ³DAMTP, University of Cambridge, Cambridge, UK. Correspondence to: Shujun Wang<shu-jun.wang@polyu.edu.hk>.

Preliminary Work.

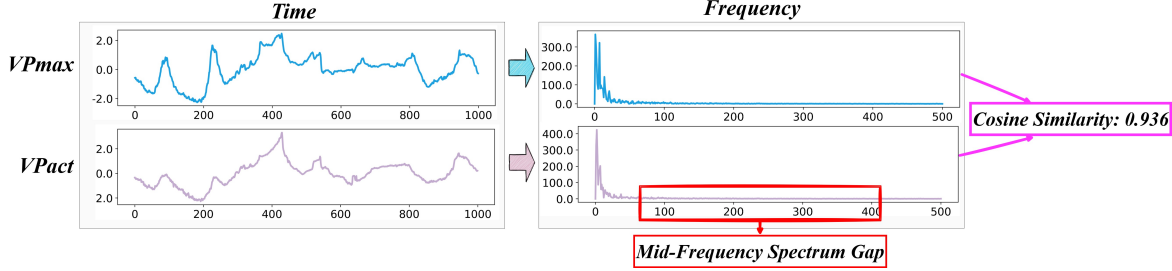


Figure 1: The **Mid-Frequency Spectrum Gap** and the shared **Key-Frequency** (high similarity in frequency spectra across variables) on Weather dataset. VPmax means ‘Maximum Vapor Pressure’ and VPact means ‘Actual Vapor Pressure’.

trum Gap and the shared Key-Frequency modeling.

- **Mid-Frequency Spectrum Gap** (Figure 1 Red box) refers to a condition where the energy of the spectrum is concentrated in the low-frequency regions, resulting in the mid-frequency band being negligible. Low-frequency components capture long-term trends, often contributing to mean shifts when overly concentrated (Stock & Watson, 2002; Granger & Newbold, 1974; Chatfield & Xing, 2019). So this Mid-Frequency Spectrum Gap will introduce **Nonstationarity** (Cheng et al., 2015; Liu et al., 2022c), where the mean and variance of time series change over time, and make time series less predictable. Furthermore, such uneven energy distribution challenges existing deep-learning models to extract critical patterns (Tishby & Zaslavsky, 2015; Xu et al., 2024b; Rahaman et al., 2019). So, addressing this Mid-Frequency Spectrum Gap is crucial for enhancing the feature extraction capabilities of deep learning-based forecasters (Park et al., 2019; Bai et al., 2018; Guo et al., 2019). Currently, widely used methods for processing spectra, such as Filters (Asselin, 1972), and **RevIN** (Kim et al., 2022; Liu et al., 2022c)—a technique previously applied to address non-stationarity—are not effective in resolving this issue. Conversely, convolution with residual connections has effectively handled spectral information (Can & Timofte, 2018; Chakraborty & Trehan, 2021), providing a potential solution.
- Meanwhile, the second challenge: the shared **Key-Frequency Modeling** (Figure 1 Pink box) has the disadvantage that distinct time series can exhibit indistinguishable frequency patterns, potentially leading to challenges in accurately differentiating and analyzing individual series within a multivariate context (Yu et al., 2023; Piao et al., 2024). However, existing approaches have largely overlooked this critical characteristic. Meanwhile, energy, which is the square of the amplitude of the spectrum, is proven as an effective tool for identifying certain frequency patterns in the multivariate case (Bogalo et al., 2024; Chekroun &

Kondrashov, 2017; Sundararajan & Bruce, 2023).

Based on the above observations, this work mainly addresses two critical questions: (1) How can the Mid-Frequency Spectrum Gap be resolved to achieve a more evenly dispersed spectrum? (2) How can inter-series dependencies be efficiently modeled by leveraging the shared Key-Frequency? To tackle challenge 1, we propose the ‘Adaptive Mid-Frequency Energy Optimizer’ (AMEO), a convolution- and residual learning-based solution. It adaptively scales the frequency spectrum by assigning higher scaling factors to lower frequencies, thereby dispersing the spectrum. To address challenge 2, For the second challenge, we introduce the ‘Energy-based Key-Frequency Picking Block (EKPB)’, which features fewer parameters and faster inference speeds compared to the Transformer Encoder (Liu et al., 2024b) and MLP-Mixer (Chen et al., 2023). EKPB extracts shared frequency information across channels effectively. We also propose a ‘Key-Frequency Enhanced Training’ strategy (KET) which incorporates spectral information from other channels during training to enhance extraction of shared Key-Frequency that may not be included in the training set.

Our contributions are summarized as follows.

- We theoretically and empirically demonstrate that existing RevIN and high/low-pass filters fail to address the Mid-Frequency Spectrum Gap. We propose AMEO, a novel approach based on convolution and residual learning that significantly enhances mid-frequency feature extraction.
- We propose EKPB to capture shared Key-Frequency across channels, which achieves superior inter-series modeling capacity with lower parameters.
- We propose KET, where spectral information from other channels is randomly introduced into each channel, to enhance the extraction of the shared Key-Frequency.
- Our approach outperforms the previous SOTA iTTransformer by reducing MSE by 4%, 6%, and 5% on the challenging Traffic, ECL, and Solar datasets, respectively, establishing new benchmarks in multivariate time series forecasting.

2. Related work

Advancement in Recent Deep Learning-based Time Series Forecasting Recent advancements in deep learning-based time series forecasting can be broadly categorized into three key areas: (1) the application of sequential models to time series data, (2) the tokenization of time series, and (3) the exploration of intrinsic patterns within time series. Efforts in the first area have focused on deploying various architectures for time series forecasting, including Transformer (Wu et al., 2021; Wang et al., 2024b), Mamba (Ahamed & Cheng, 2024; Wang et al., 2024d), MLPs (Wang et al., 2024a; Das et al., 2023; Yu et al., 2024a), RNNs (Lin et al., 2023), Graph Neural Networks (Shang et al., 2024), TCNs (Wang et al., 2023), and even Large Language Models (LLMs) (Jin et al., 2024; Liu et al., 2024d;c). The second direction has witnessed groundbreaking developments, particularly in Patch Embedding (Nie et al., 2023) and Variate Embedding (Liu et al., 2024b). The final area explores modeling complex relationships, including the inter-series dependencies (Ng et al., 2022; Chen et al., 2024), the dynamic evolution within a sequence (Du et al., 2023; Zhang et al., 2022), or both (Yu et al., 2024b; Liu et al., 2024a).

Time Series Modeling with Frequency Frequency as a key feature of time series data, has inspired numerous works (Yi et al., 2023a). FITS (Xu et al., 2024a) employs a simple frequency-domain linear, getting results comparable to SOTA models with 10K parameters. Autoformer (Wu et al., 2021) introduces the auto-correlation mechanism, leveraging FFT to improve self-attention. FEDformer (Zhou et al., 2022c) further calculates attention weights from the spectrum of queries and keys. FiLM (Zhou et al., 2022b) applies Fourier analysis to preserve historical information while filtering out noise. FreTS (Yi et al., 2023c) incorporates frequency-domain MLP to model both channel and temporal dependencies. TimesNet (Wu et al., 2023) utilizes FFT to extract periodic patterns. FilterNet (Yi et al., 2024) proposes a filter-based method from the perspective of signal processing.

However, they do not address the Mid-Frequency Spectrum Gap and shared Key-Frequency modeling. In contrast, our method employs ‘Adaptive Mid-Frequency Energy Optimizer’ to improve mid-frequency feature extraction and introduces ‘Energy-based Key-Frequency Picking Block’ with ‘Key-Frequency Enhanced Training’ strategy to capture shared Key-Frequency across channels.

3. Methodology

3.1. Problem Definition

Given a multivariate time series input $X \in \mathbb{R}^{C \times T}$, multivariate time series forecasting tasks are designed to predict

its future F time steps $\hat{Y} \in \mathbb{R}^{C \times F}$ using past T steps. C is the number of variates or channels.

3.2. Preliminary Analysis

This section presents why RevIN (Kim et al., 2022; Liu et al., 2022c), High-pass, and Low-pass filters fail to address the Mid-Frequency Spectrum Gap. Let the input univariate time series be $x(t)$ with length T and target $y(t)$ with length F .

Definition 3.1 (Frequency Spectral Energy). The Fourier transform of $x(t)$, $X(f)$, and its spectral energy $E_X(f)$ is given by:

$$X(f) = \sum_{t=0}^{T-1} x(t) e^{-i2\pi ft/T}, \quad f = 0, 1, \dots, T-1$$

$$E_X(f) = |X(f)|^2. \quad (1)$$

Impact of RevIN on Frequency Spectrum

Definition 3.2 (Reversible Instance Normalization). Given a **forecast model** $f : \mathbb{R}^T \rightarrow \mathbb{R}^F$ that generates a forecast $\hat{y}(t)$ from a given input $x(t)$, RevIN is defined as:

$$\hat{x}(t) = \frac{x(t) - \mu}{\sigma}, \quad t = 0, 1, \dots, T-1$$

$$\hat{y}(t) = f(\hat{x}(t)), \quad \hat{y}(t)_{rev} = \hat{y}(t) \cdot \sigma + \mu,$$

$$\mu = \frac{1}{T} \sum_{t=0}^{T-1} x(t), \quad \sigma = \sqrt{\frac{1}{T} \sum_{t=0}^{T-1} (x(t) - \mu)^2}. \quad (2)$$

Theorem 3.3 (Frequency Spectrum after RevIN). *The spectral energy of $\hat{x}(t)$ (transformed using RevIN):*

$$E_{\hat{X}}(0) = 0, \quad f = 0,$$

$$E_{\hat{X}}(f) = \left(\frac{1}{\sigma}\right)^2 |X(f)|^2, \quad f = 1, 2, \dots, T-1. \quad (3)$$

The proof is in Appendix A.1. Theorem 3.3 suggests that RevIN scales the absolute spectral energy by σ^2 but does not affect its relative distribution except $E_{\hat{X}}(0) = 0$. Thus, RevIN preserves the relative spectral energy distribution and leaves the Mid-Frequency Spectrum Gap unresolved. *However, our experiments still employ RevIN to ensure a fair comparison with other baselines.*

Impact of High- and Low-pass filter We still define $\hat{x}(t)$ to be the filtered (processed) signal, obtained by applying a filter $H(f)$ (High/Low-pass filter). The filter $H(f)$ is 1 in the passband (High/Low frequency) and 0 in the stopband (Middle frequency). So $E_{\hat{X}}(f) = 0, \quad E_{\hat{X}} \leq E_X(f)$ for middle frequencies, which creates even larger gap.

3.3. Overall Structure of The Proposed ReFocus

In this section, we elucidate the overall architecture of **ReFocus**, depicted in Figure 2. We define frequency domain

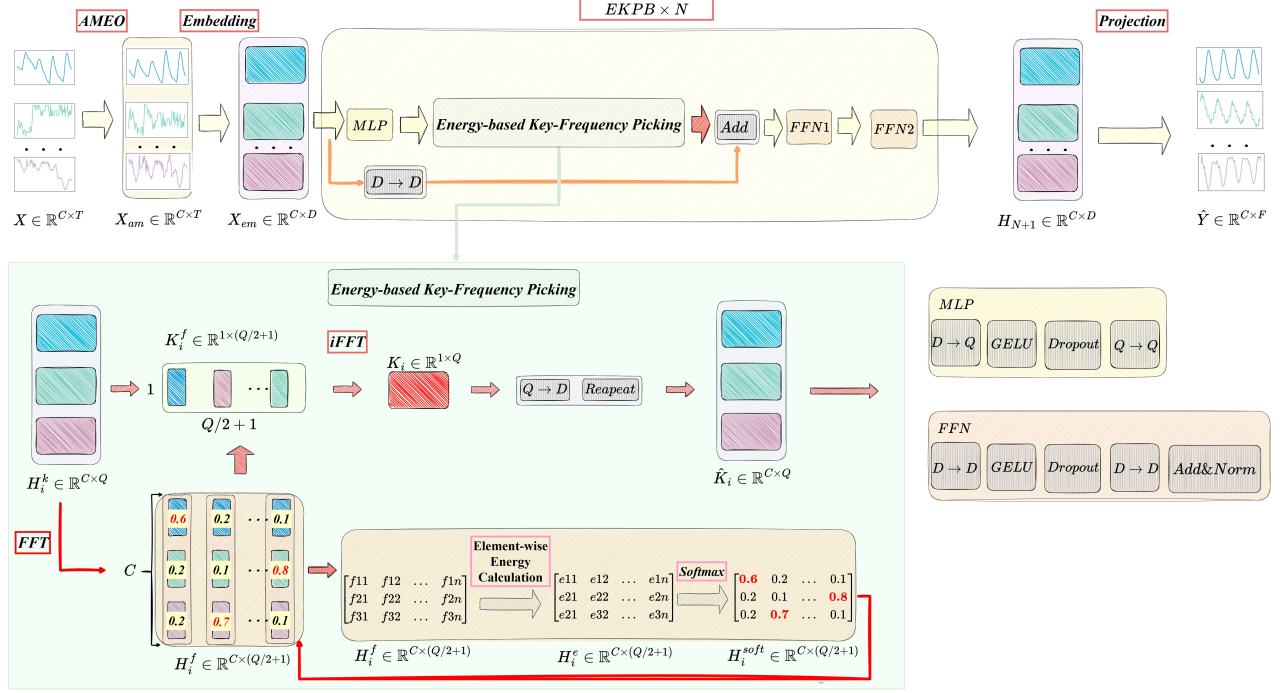


Figure 2: General structure of **ReFocus**. ‘Adaptive Mid-Frequency Energy Optimizer (AMEO)’ enhances mid-frequency components modeling, and ‘Energy-based Key-Frequency Picking Block’ (EKPB) effectively captures shared Key-Frequency across channels

projection as $D1 \rightarrow D2$ representing a projection from dimension $D1$ to $D2$ in the frequency domain (Xu et al., 2024a). Initially, we apply AMEO to the input $X \in \mathbb{R}^{C \times T}$, yielding the processed spectrum $X_{am} \in \mathbb{R}^{C \times T}$. Next, we use a projection $T \rightarrow D$ to transform X_{am} into the Variate Embedding $X_{em} \in \mathbb{R}^{C \times D}$ (Liu et al., 2024b). Then, X_{em} go through N EKPB to generate representation H_{N+1} , which is projected to obtain final prediction \hat{Y} .

Adaptive Mid-Frequency Energy Optimizer Building upon the **Preliminary Analysis**, we propose a convolution- and residual learning-based solution to address the Mid-Frequency Spectrum Gap, which we denoted as AMEO.

Definition 3.4 (Adaptive Mid-Frequency Energy Optimizer). AMEO is defined as:

$$\begin{aligned} \hat{x}(t) &= x(t) - \frac{\beta}{K} \sum_{k=0}^{K-1} \tilde{x}(t+K-1-k), \\ \tilde{x}(t) &= \begin{cases} x(t - (\frac{K}{2} + 1)), & \text{if } \frac{K}{2} + 1 \leq t < T + \frac{K}{2} + 1, \\ 0, & \text{if } 0 \leq t < \frac{K}{2} + 1 \text{ or } T + \frac{K}{2} + 1 \leq t < T + K. \end{cases} \end{aligned} \quad (4)$$

It is equivalent to $x = x - \beta \cdot \text{Conv}(x)$. Conv is a 1D convolution (Zero-padding at both ends, stride $s = 1$, kernel size K , with values initialized as $\frac{1}{K}$). $\beta \in \mathbb{R}^1$ is a hyperparameter.

Theorem 3.5 (Frequency Spectrum after AMEO). *The spectral energy of $\hat{x}(t)$ obtained using AMEO:*

$$E_{\hat{x}}(f) = |X(f)|^2 \left\{ 1 - \beta \cdot \underbrace{\frac{1}{K} \sum_{k=0}^{K-1} e^{i2\pi f(\frac{3K}{2} - k - 2)/T - 1}}_{G(f)} \right\}^2 \quad (5)$$

The proof is in Appendix A.2. We have $E_{\hat{x}}(f) = |X(f)|^2(1 - \beta \cdot G(f))^2$. Generally, $G(f)$ behaves as a decay function, gradually reducing its value from **One** to **Zero**. Such **decay behavior** makes AMEO relatively enhances mid-frequency components, thus addressing the Mid-Frequency Spectrum Gap.

Energy-based Key-Frequency Picking Block In each EKPB, the input $H_i \in \mathbb{R}^{C \times D}$ ($H_1 = X_{em}$) is first processed through an MLP to generate $H_i^k \in \mathbb{R}^{C \times Q}$. Then, FFT is applied to get $H_i^f \in \mathbb{R}^{C \times (Q/2+1)}$. For H_i^f , we calculate its energy, denoted as $H_i^e \in \mathbb{R}^{C \times (Q/2+1)}$. A cross-channel softmax is then applied to H_i^e per frequency to obtain a probability distribution $H_i^{soft} \in \mathbb{R}^{C \times (Q/2+1)}$.

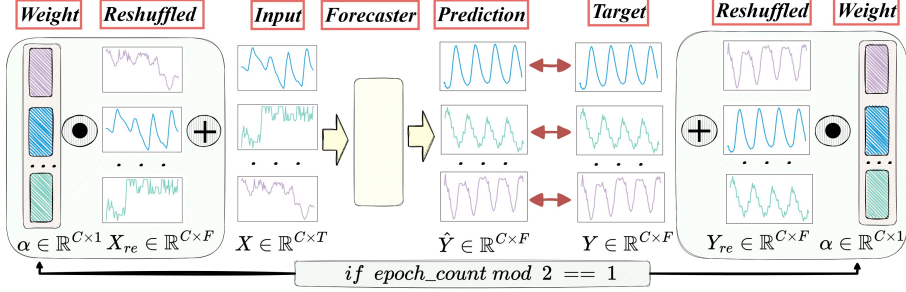


Figure 3: General process of the **Key-Frequency Enhanced Training strategy (KET)**, where spectral information from other channels is randomly introduced into each channel, to enhance the extraction of the shared Key-Frequency.

Using H_i^{soft} , we select values from H_i^f across channels for each frequency, resulting in $K_i^f \in \mathbb{R}^{1 \times (Q/2+1)}$, which represents the Shared Key-Frequency across all channels. Then iFFT is performed on K_i^f to get $K_i \in \mathbb{R}^{1 \times Q}$, followed by projection $Q \rightarrow D$ and repeating (C times) to get $\hat{K}_i \in \mathbb{R}^{C \times D}$. This \hat{K}_i is point-wisely added to $\hat{H}_i \in \mathbb{R}^{C \times D}$, which is the projection of H_i using projection $D \rightarrow D$. Then, an MLP and *Add&Norm* is applied to the result $HK \in \mathbb{R}^{C \times D}$ to fuse inter-series dependencies information, and another MLP and *Add&Norm* is used to capture intra-series variations (Liu et al., 2024b). The output of each **EKPB** is $\hat{O}_i \in \mathbb{R}^{C \times D}$, where $H_{i+1} = \hat{O}_i$.

3.4. Key-Frequency Enhanced Training strategy

In real-world time series, certain channels often exhibit spectral dependencies, which may not be fully captured in the training set, and the specific channels with such dependencies are also unknown (Geweke, 1984; Zhao & Shen, 2024). So this work borrows insight from recent advancement of mix-up in time series (Zhou et al., 2023; Ansari et al., 2024), randomly introducing spectral information from other channels into each channel, to enhance the extraction of the shared Key-Frequency, as in Figure 3. Given a multivariate time series input $X \in \mathbb{R}^{C \times T}$ and its ground-truth $Y \in \mathbb{R}^{C \times F}$, we generate a pseudo sample pair:

$$\begin{aligned} X' &= iFFT(FFT(X) + \alpha \cdot FFT(X[\text{perm}, :])), \\ Y' &= iFFT(FFT(Y) + \alpha \cdot FFT(Y[\text{perm}, :])). \end{aligned} \quad (6)$$

$\alpha \in \mathbb{R}^{C \times 1}$ is a weight vector sampled from a normal distribution, perm is a reshuffled channel index. Since FFT and $iFFT$ are linear operations, this mix-up process can be equivalently simplified in the **Time Domain**:

$$\begin{aligned} X' &= X + \alpha \cdot X[\text{perm}, :], \\ Y' &= Y + \alpha \cdot Y[\text{perm}, :] \end{aligned} \quad (7)$$

We alternate training between real and synthetic data to preserve the spectral dependencies in real samples. This

combines the advantages of data augmentation, such as improved generalization, while mitigating potential drawbacks like over-smoothing and training instability (Ryu et al., 2024; Alkhaliifah et al., 2022).

4. Experiments

4.1. Experimental Settings

This section first introduces the whole experiment settings under a fair comparison. Secondly, we illustrate the experiment results by comparing **ReFocus** with the **TEN** well-acknowledged baselines. Further, we conducted an ablation study to comprehensively investigate the effectiveness of the ‘Adaptive Mid-Frequency Energy Optimizer’ (AMEO), ‘Energy-based Key-Frequency Picking Block’ (EKPB), and ‘Key-Frequency Enhanced Training strategy’ (KET).

Table 1: The Statistics of the eight datasets used in our experiments.

Datasets	ETTh1&2	ETTm1&2	Traffic	Electricity	Solar_Energy	Weather
Variates	7	7	862	321	137	21
Timesteps	17,420	69,680	17,544	26,304	52,560	52,696
Granularity	1 hour	5 min	1 hour	1 hour	10 min	10 min

Datasets We conduct extensive experiments on selected **Eight** widely-used real-world multivariate time series forecasting datasets, including Electricity Transformer Temperature (ETTh1, ETTh2, ETTm1, and ETTm2), Electricity, Traffic, Weather used by Autoformer (Wu et al., 2021), and Solar_Energy datasets proposed in LSTNet (Lai et al., 2018). For a fair comparison, we follow the same standard protocol (Liu et al., 2024b) and split all forecasting datasets into training, validation, and test sets by the ratio of 6:2:2 for the ETT dataset and 7:1:2 for the other datasets. The characteristics of these datasets are shown in Table 1 (More can be found in the Appendix).

Evaluation protocol Following TimesNet (Wu et al., 2023), we use Mean Squared Error (MSE) and Mean Absolute Error (MAE) for the evaluation. We follow the same

evaluation protocol, where the input length is set as $T = 96$ and the forecasting lengths $F \in \{96, 192, 336, 720\}$. All the experiments are conducted on a single NVIDIA GeForce RTX 4090 with 24G VRAM. The MSE loss function is utilized for model optimization. To foster reproducibility, we make our code, and training scripts available in this [GitHub Repository](#)¹. Full implementation details and other information are in Appendix B.

Baseline setting We carefully choose TEN well-acknowledged forecasting models as our baselines, including 1) Transformer-based methods: iTransformer (Liu et al., 2024b), Crossformer (Zhang & Yan, 2023), PatchTST (Nie et al., 2023); 2) Linear-based methods: TSMixer (Chen et al., 2023), DLinear (Zeng et al., 2023); 3) TCN-based methods: TimesNet (Wu et al., 2023), ModernTCN (Donghao & Xue, 2024); 4) Recent cutting-edge frequency-based methods that discussed earlier: FilterNet (Yi et al., 2024), FITS (Xu et al., 2024a), FreTS (Yi et al., 2023c). These models represent the latest advancements in multivariate time series forecasting and encompass all mainstream prediction model types. The results of ModernTCN, FilterNet, FITS, and FreTS are taken from FilterNet (Yi et al., 2024) and other results are taken from iTransformer (Liu et al., 2024b).

4.2. Experiment Results

Quantitative comparison Comprehensive forecasting results are listed in Table 2. We leave full forecasting results in APPENDIX to save place. It is quite evident that **ReFocus** has demonstrated superior predictive performance across all datasets, significantly outperforming the second-best method. Especially, Compared to the previous SOTA **iTransformer**, we have reduced the MSE by **4%, 6%, and 5%** on the three most challenging benchmarks: Traffic, ECL, and Solar, respectively, indicating a significant breakthrough. These significant improvements indicate that the **ReFocus** model possesses robust performance and broad applicability in multivariate time series forecasting tasks, especially in tasks with a large number of channels, such as the Solar_Energy dataset (**137** channels), ECL dataset (**321** channels), and Traffic dataset (**862** channels).

4.3. Model Analysis

Ablation study of AMEO and KET To evaluate the contributions of each module in ReFocus, we performed ablation studies on the ‘Adaptive Mid-Frequency Energy Optimizer (AMEO)’ and the ‘Key-Frequency Enhanced Training (KET)’ strategy. The results are summarized in Table 3. Notably, integrating both modules achieves the best performance, highlighting the effectiveness of their

synergy. Additionally, each module delivers substantial improvements over baseline models in most cases.

Further study of KET We conducted further ablation studies on the KET to demonstrate the importance of alternate training between real and synthetic data. The experimental results in Table 4 reveal that while training on pseudo samples can partially enhance the model’s generalization performance on the test set, it also tends to cause over-smoothing and training instability on more complex datasets, such as Solar_Energy. In contrast, training on real and synthetic data alternatively (KET) improves generalization and mitigates over-smoothing and training instability by preserving the spectral dependencies of real samples. More Analyses are in Appendix C.

Ablation study of different Key-Frequency Picking strategy We conducted an ablation study on various key-frequency selection strategies. The evaluated methods include Maximum-based, Minimum-based, and **Softmax-based** random sampling strategies. Our experimental results in Table 5 reveal that purely relying on Maximum or Minimum-based strategies may overlook certain critical Key-Frequency. In contrast, the random sampling strategy based on a Softmax probabilistic distribution consistently achieved the best overall performance, particularly on datasets with a larger number of channels and higher complexity—key challenges in multivariate time series forecasting.

Outstanding inter-series modeling ability of the EKPB We compared ‘Energy-based Key-Frequency Picking Block’ (EKPB) with several well-established backbones, including iTransformer (Liu et al., 2024b), TSMixer (Chen et al., 2023), and Crossformer (Zhang & Yan, 2023), which have demonstrated exceptional performance in modeling inter-series dependencies. Additionally, we included FECAM (Jiang et al., 2023), a method also designed for modeling cross-channel frequency-domain dependencies. The results presented in Table 6 demonstrate that our EKPB outperforms in modeling inter-series dependencies across multiple datasets. Additionally, when comparing the number of parameters and inference time during prediction under identical configurations on the ECL dataset, our EKPB method still outperforms other baselines by a significant margin, as in Table 7. To illustrate EKPB’s functionality, we visualize the series embeddings with and without its adjustment in Figure 5. The T-SNE visualization of the series embeddings shows that without EKPB, using only the channel-independent strategy (Nie et al., 2023), the MSE is 0.171. After applying EKPB, channels sharing Key-Frequency (variates 2&3) are clustered, while others (variates 1&3) are separated. This adjustment improves the MSE from 0.171 to 0.145, a **15%** reduction. These indicate that EKPB not only achieves better predictive performance

¹<https://github.com/Levi-Ackman/ReFocus>

Table 2: Multivariate forecasting results with prediction lengths $F \in \{96, 192, 336, 720\}$ and fixed lookback length $T = 96$. Results are averaged from all prediction lengths. The best is **Red** and the second is **Blue**. The **Lower** MSE/MAE indicates the better prediction result. Full results are in Appendix D.

Models	ReFocus (Ours)	FilterNet (2024)	iTransformer (2024b)	ModernTCN (2024)	FITS (2024a)	PatchTST (2023)	Crossformer (2023)	TimesNet (2023)	TSMixer (2023)	DLinear (2023)	FreTS (2023c)	
Metric	MSE	MAE	MSE	MAE	MSE	MAE	MSE	MAE	MSE	MAE	MSE	MAE
ETTm1	0.387 0.394	0.392 0.401	0.407 0.410	0.389 0.402	0.415 0.408	0.387 0.400	0.513 0.496	0.400 0.406	0.398 0.407	0.403 0.407	0.408 0.416	
ETTm2	0.275 0.320	0.285 0.328	0.288 0.332	0.279 0.322	0.286 0.328	0.281 0.326	0.757 0.610	0.291 0.333	0.289 0.333	0.350 0.401	0.321 0.368	
ETTh1	0.434 0.433	0.441 0.439	0.454 0.447	0.446 0.433	0.451 0.440	0.469 0.454	0.529 0.522	0.458 0.450	0.463 0.452	0.456 0.452	0.475 0.463	
ETTh2	0.371 0.396	0.383 0.407	0.383 0.407	0.382 0.404	0.383 0.408	0.387 0.407	0.942 0.684	0.414 0.427	0.401 0.417	0.559 0.515	0.472 0.465	
ECL	0.168 0.262	0.173 0.268	0.178 0.270	0.197 0.282	0.217 0.295	0.205 0.290	0.244 0.334	0.192 0.295	0.186 0.287	0.212 0.300	0.189 0.278	
Traffic	0.412 0.265	0.463 0.310	0.428 0.282	0.546 0.348	0.627 0.376	0.481 0.304	0.550 0.304	0.620 0.336	0.522 0.357	0.625 0.383	0.618 0.390	
Weather	0.245 0.271	0.245 0.272	0.258 0.279	0.247 0.272	0.249 0.276	0.259 0.281	0.259 0.315	0.259 0.287	0.256 0.279	0.265 0.317	0.250 0.270	
Solar_Energy	0.222 0.252	0.243 0.281	0.233 0.262	0.244 0.286	0.395 0.407	0.270 0.307	0.641 0.639	0.301 0.319	0.260 0.297	0.330 0.401	0.248 0.296	

Table 3: Ablation of ‘Adaptive Mid-Frequency Energy Optimizer (AMEO)’ and ‘Key-Frequency Enhanced Training strategy (KET)’. We list the average results. Full results are in Appendix D.

AMEO	KET	ETTm1	ETTm2	ETTh1	ETTh2	ECL	Traffic	Weather	Solar_Energy		
		MSE	MAE								
-	-	0.401	0.403	0.283	0.325	0.440	0.437	0.376	0.400	0.178	0.270
-	✓	0.394	0.396	0.279	0.322	0.437	0.435	0.373	0.398	0.171	0.263
✓	-	0.393	0.402	0.282	0.326	0.443	0.440	0.372	0.397	0.174	0.267
✓	✓	0.387	0.394	0.275	0.320	0.434	0.433	0.371	0.396	0.168	0.262
		0.412	0.265	0.428	0.282	0.546	0.348	0.627	0.376	0.481	0.304

Table 4: Further ablation of ‘Key-Frequency Enhanced Training strategy (KET)’. ‘Real’ means KET is not performed, i.e. trained on original data. ‘Pseudo’ means trained on Pseudo samples. If both are used (Bottom Line), this means the model is trained on Real and Pseudo samples alternatively, i.e. **KET**. We list the average results. Full results are in Appendix D.

Real	Pseudo	ETTm1	ETTm2	ETTh1	ETTh2	ECL	Traffic	Weather	Solar_Energy		
		MSE	MAE								
✓	-	0.401	0.403	0.283	0.325	0.440	0.437	0.376	0.400	0.178	0.270
-	✓	0.396	0.398	0.280	0.323	0.436	0.434	0.372	0.397	0.175	0.266
✓	✓	0.394	0.396	0.279	0.322	0.437	0.435	0.373	0.398	0.171	0.263

Table 5: Ablation study of different Key-Frequency Picking strategies. ‘Softmax’ means using softmax function to generate a probability distribution and picking shared Key-Frequency using this distribution. ‘Max’ means always choosing the biggest energy. ‘Min’ means always choosing the smallest energy. We list the average results. Full results are in Appendix D.

Picking Strategy	ETTm1	ETTm2	ETTh1	ETTh2	ECL	Traffic	Weather	Solar_Energy				
	MSE	MAE	MSE	MAE	MSE	MAE	MSE	MAE				
Min	0.388	0.392	0.280	0.323	0.432	0.432	0.371	0.396	0.194	0.281	0.517	0.344
Max	0.392	0.395	0.279	0.322	0.437	0.435	0.374	0.398	0.172	0.265	0.422	0.273
Softmax	0.387	0.394	0.275	0.320	0.434	0.433	0.371	0.396	0.168	0.262	0.412	0.265

but also offers a more resource-efficient solution than other baselines.

Superiority of AMEO over RevIN and Filters We investigated the roles of AMEO, RevIN, and Filters in addressing the Mid-Frequency Spectrum Gap through time-frequency domain visualization analysis. The results presented in Figure 4 align perfectly with our theoretical anal-

ysis before. High-pass and low-pass filters fail to address the Mid-Frequency Spectrum Gap and exacerbate this issue. RevIN, on the other hand, merely eliminates the energy of the zero-frequency component while scaling other components using the variance σ^2 , which also does not effectively resolve the problem. In contrast, our AMEO successfully amplifies the mid-frequency energy. Furthermore, compared to the original sequence and the sequence processed by

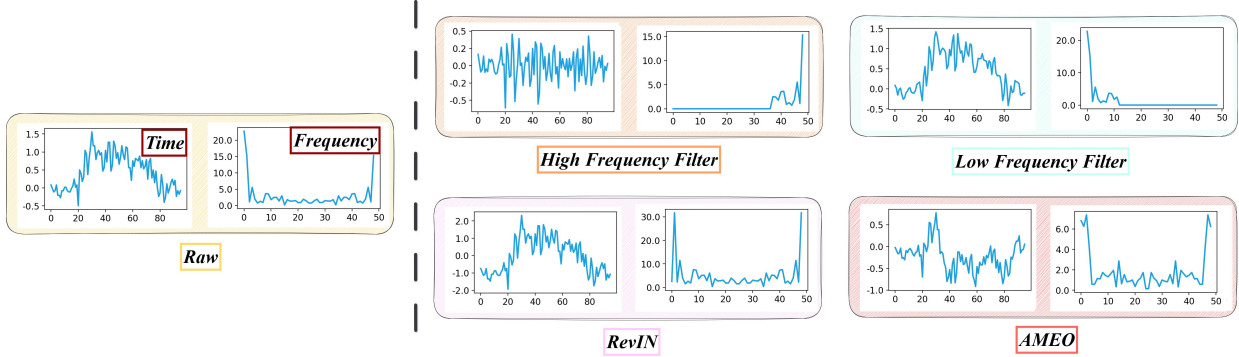


Figure 4: The time-frequency domain visualization of the original sequence (ETTm1, *the last variate*), the sequence processed by high-pass and low-pass filters, by RevIN, and by AMEO. We selected the *input* – 96 – *forecast* – 96 task.

Table 6: Multivariate forecasting result of ‘Energy-based Key-Frequency Picking Block’ (EKPB) and other inter-series dependencies modeling backbones. * means ‘former.’ We list the average results. Full results are in Appendix D.

Dataset	EKPB	TSMixer	iTrans*	Cross*	FECAM	
	MSE	MAE	MSE	MAE	MSE	MAE
ETTm2	0.282	0.324	0.289	0.333	0.288	0.332
ETTh2	0.374	0.399	0.401	0.417	0.383	0.407
Weather	0.252	0.277	0.256	0.279	0.258	0.279
ECL	0.176	0.268	0.186	0.287	0.178	0.270

Table 7: Model efficiency analysis. We evaluated the **parameter count**, and the **inference time** (average of 5 runs on a single NVIDIA 4090 24GB GPU) with *batch_size* = 1 on **ECL** dataset. We set the dimension of layer *dim* ∈ {256, 512}, and the number of network layers *N* = 2. The task is **input-96-forecast-720**. * means ‘former.’ **Para** means ‘Parameter count(M).’ **Time** means ‘inference time(ms).’

Dim	EKPB	Cross*	iTrans*	TSMixer	FECAM	
	Param	Time	Para	Time	Para	Time
256	0.29	68.91	0.93	98.37	1.27	192.12
512	0.97	84.54	1.78	118.29	4.63	249.60

Table 8: Experiment result of high-pass filter, low-pass filter, RevIN, and AMEO using a **simple linear projection** as the forecaster on Weather and ETTm1 dataset. We set the input length *T* = 96 and forecasting length *F* ∈ {720, 96}.

Dataset	Length	AMEO	RevIN	Low	High	None	
		MSE	MAE	MSE	MAE	MSE	MAE
ETTm1	96	0.331	0.365	0.354	0.375	0.345	0.371
	720	0.466	0.440	0.486	0.448	0.478	0.458
Weather	96	0.164	0.236	0.194	0.234	0.198	0.258
	720	0.331	0.370	0.365	0.353	0.353	0.387

RevIN, we observe that the sequence processed by AMEO exhibits significantly higher stationarity with much more stable means and variance.

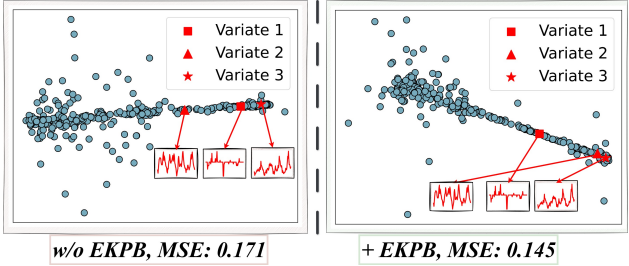


Figure 5: T-SNE visualization of the series embeddings with and without ‘Energy-based Key-Frequency Picking Block’ (EKPB) on ECL dataset. We choose the *input* – 96 – *forecast* – 96 task. Three example variates are highlighted: variates 2&3 shared a common Key-Frequency, while variate 1 does not.

In Table 8, the performance of AMEO on two prediction tasks across two datasets consistently surpasses the results achieved by methods based on RevIN and Filters. Furthermore, while Filters and RevIN occasionally lead to degraded performance on certain datasets, AMEO consistently delivers results that outperform the original methods. These findings further highlight the superiority of AMEO over alternative approaches.

5. Conclusion

This work addresses two critical challenges in multivariate time series forecasting: the Mid-Frequency Spectrum Gap and the efficient modeling of the shared Key-Frequency. We propose the ‘Adaptive Mid-Frequency Energy Optimizer’, which effectively enhances mid-frequency extraction, and the ‘Energy-based Key-Frequency Picking Block’ with the ‘Key-Frequency Enhanced Training’ strategy, which efficiently captures shared frequency patterns. Extensive experiments demonstrate the superiority of our approach, achieving up to 6% MSE reduction on challenging benchmarks, thus advancing the SOTA in frequency-domain forecasting.

References

- Ahamed, M. A. and Cheng, Q. Timemachine: A time series is worth 4 mambas for long-term forecasting. *arXiv preprint arXiv:2403.09898*, 2024. URL <https://arxiv.org/abs/2403.09898>.
- Alkhalifah, T., Wang, H., and Ovcharenko, O. Mlreal: Bridging the gap between training on synthetic data and real data applications in machine learning. *Artificial Intelligence in Geosciences*, 3:101–114, 2022.
- Ansari, A. F., Stella, L., Turkmen, C., Zhang, X., Mercado, P., Shen, H., Shchur, O., Rangapuram, S. S., Arango, S. P., Kapoor, S., et al. Chronos: Learning the language of time series. *arXiv preprint arXiv:2403.07815*, 2024.
- Asselin, R. Frequency filter for time integrations. *Monthly Weather Review*, 100(6):487–490, 1972.
- Bai, S., Kolter, J. Z., and Koltun, V. An empirical evaluation of generic convolutional and recurrent networks for sequence modeling. *arXiv preprint arXiv:1803.01271*, 2018.
- Bógalo, J., Poncela, P., and Senra, E. Understanding fluctuations through multivariate circulant singular spectrum analysis. *Expert Systems with Applications*, 251:123827, 2024.
- Can, Y. B. and Timofte, R. An efficient cnn for spectral reconstruction from rgb images. *arXiv preprint arXiv:1804.04647*, 2018.
- Chakraborty, T. and Trehan, U. Spectralnet: Exploring spatial-spectral waveletcnn for hyperspectral image classification. *arXiv preprint arXiv:2104.00341*, 2021.
- Chatfield, C. and Xing, H. *The analysis of time series: an introduction with R*. Chapman and hall/CRC, 2019.
- Chekroun, M. D. and Kondrashov, D. Data-adaptive harmonic spectra and multilayer stuart-landau models. *Chaos: An Interdisciplinary Journal of Nonlinear Science*, 27(9), 2017.
- Chen, J., Lenssen, J. E., Feng, A., Hu, W., Fey, M., Tasiuslas, L., Leskovec, J., and Ying, R. From similarity to superiority: Channel clustering for time series forecasting. *arXiv preprint arXiv:2404.01340*, 2024. URL <https://arxiv.org/abs/2404.01340>.
- Chen, S.-A., Li, C.-L., Arik, S. O., Yoder, N. C., and Pfister, T. Tsmixer: An all-mlp architecture for time series forecasting. *Transactions on Machine Learning Research*, 2023. ISSN 2835-8856. URL <https://openreview.net/forum?id=wbpXTuXgm0>.
- Cheng, C., Sa-Ngasoongsong, A., Beyca, O., Le, T., Yang, H., Kong, Z., and Bukkapatnam, S. T. Time series forecasting for nonlinear and non-stationary processes: a review and comparative study. *Iie Transactions*, 47(10):1053–1071, 2015.
- Cirstea, R.-G., Guo, C., Yang, B., Kieu, T., Dong, X., and Pan, S. Triformer: Triangular, variable-specific attentions for long sequence multivariate time series forecasting—full version. *arXiv preprint arXiv:2204.13767*, 2022.
- Dai, T., Wu, B., Liu, P., Li, N., Bao, J., Jiang, Y., and Xia, S.-T. Periodicity decoupling framework for long-term series forecasting. In *The Twelfth International Conference on Learning Representations*, 2024.
- Das, A., Kong, W., Leach, A., Mathur, S. K., Sen, R., and Yu, R. Long-term forecasting with tide: Time-series dense encoder. *Transactions on Machine Learning Research*, 2023. ISSN 2835-8856. URL <https://openreview.net/forum?id=pCbC3aQB5W>.
- Dong, J., Wu, H., Zhang, H., Zhang, L., Wang, J., and Long, M. Simmtm: A simple pre-training framework for masked time-series modeling. In *Proceedings of the Thirty-seventh Conference on Neural Information Processing Systems*, 2023. URL <https://openreview.net/forum?id=ginTcBUnL8>.
- Donghao, L. and Xue, W. Moderntcn: A modern pure convolution structure for general time series analysis. In *Proceedings of the Twelfth International Conference on Learning Representations*, 2024. URL <https://openreview.net/forum?id=vpJMJerXHU>.
- Du, D., Su, B., and Wei, Z. Preformer: Predictive transformer with multi-scale segment-wise correlations for long-term time series forecasting. In *ICASSP 2023-2023 IEEE International Conference on Acoustics, Speech and Signal Processing (ICASSP)*. IEEE, 2023.
- Eldele, E., Ragab, M., Chen, Z., Wu, M., and Li, X. Tslanet: Rethinking transformers for time series representation learning. In *International Conference on Machine Learning*, 2024.
- Fan, W., Yi, K., Ye, H., Ning, Z., Zhang, Q., and An, N. Deep frequency derivative learning for non-stationary time series forecasting. *arXiv preprint arXiv:2407.00502*, 2024.
- Geweke, J. F. Measures of conditional linear dependence and feedback between time series. *Journal of the American Statistical Association*, 79(388):907–915, 1984.
- Granger, C. W. and Newbold, P. Spurious regressions in econometrics. *Journal of econometrics*, 2(2):111–120, 1974.

- Guo, H., Mao, Y., and Zhang, R. Mixup as locally linear out-of-manifold regularization. In *Proceedings of the AAAI conference on artificial intelligence*, volume 33, pp. 3714–3722, 2019.
- Han, L., Chen, X.-Y., Ye, H.-J., and Zhan, D.-C. Softs: Efficient multivariate time series forecasting with series-core fusion. *arXiv preprint arXiv:2404.14197*, 2024. URL <https://arxiv.org/abs/2404.14197>.
- Jiang, M., Zeng, P., Wang, K., Liu, H., Chen, W., and Liu, H. Fecam: Frequency enhanced channel attention mechanism for time series forecasting. *Advanced Engineering Informatics*, 58:102158, 2023.
- Jin, M., Wang, S., Ma, L., Chu, Z., Zhang, J. Y., Shi, X., Chen, P.-Y., Liang, Y., Li, Y.-F., Pan, S., and Wen, Q. Time-LLM: Time series forecasting by reprogramming large language models. In *Proceedings of the Twelfth International Conference on Learning Representations (ICLR)*, 2024. URL <https://openreview.net/forum?id=Unb5CVpta>.
- Kim, T., Kim, J., Tae, Y., Park, C., Choi, J.-H., and Choo, J. Reversible instance normalization for accurate time-series forecasting against distribution shift. In *International Conference on Learning Representations*, 2022. URL <https://openreview.net/forum?id=cGDAkQo1C0p>.
- Lai, G., Chang, W.-C., Yang, Y., and Liu, H. Modeling long-and short-term temporal patterns with deep neural networks. In *Proceedings of the 41st International ACM SIGIR Conference on Research & Development in Information Retrieval*, pp. 95–104, 2018.
- Li, Z., Qi, S., Li, Y., and Xu, Z. Revisiting long-term time series forecasting: An investigation on linear mapping. *arXiv preprint arXiv:2305.10721*, 2023.
- Lim, B. and Zohren, S. Time series forecasting with deep learning: A survey. *Philosophical Transactions of the Royal Society A: Mathematical, Physical and Engineering Sciences*, pp. 20200209, 2021. doi: 10.1098/rsta.2020.0209. URL <http://dx.doi.org/10.1098/rsta.2020.0209>.
- Lin, S., Lin, W., Wu, W., Zhao, F., Mo, R., and Zhang, H. Segrrnn: Segment recurrent neural network for long-term time series forecasting. *arXiv preprint arXiv:2308.11200*, 2023. URL <https://arxiv.org/abs/2308.11200>.
- Liu, J., Liu, C., Woo, G., Wang, Y., Hooi, B., Xiong, C., and Sahoo, D. Unitst: Effectively modeling inter-series and intra-series dependencies for multivariate time series forecasting. *arXiv preprint arXiv:2406.04975*, 2024a. URL <https://arxiv.org/abs/2406.04975>.
- Liu, M., Zeng, A., Chen, M., Xu, Z., Lai, Q., Ma, L., and Xu, Q. Scinet: Time series modeling and forecasting with sample convolution and interaction. In Oh, A. H., Agarwal, A., Belgrave, D., and Cho, K. (eds.), *Advances in Neural Information Processing Systems*, 2022a. URL <https://openreview.net/forum?id=AyajSjTAzmg>.
- Liu, S., Yu, H., Liao, C., Li, J., Lin, W., Liu, A. X., and Dusdar, S. Pyraformer: Low-complexity pyramidal attention for long-range time series modeling and forecasting. In *International Conference on Learning Representations*, 2022b. URL <https://openreview.net/forum?id=0EXmFzUn5I>.
- Liu, Y., Wu, H., Wang, J., and Long, M. Non-stationary transformers: Exploring the stationarity in time series forecasting. In *Advances in Neural Information Processing Systems*, 2022c. URL <https://openreview.net/forum?id=ucNDIDRNjjv>.
- Liu, Y., Hu, T., Zhang, H., Wu, H., Wang, S., and Long, M. itransformer: Inverted transformers are effective for time series forecasting. In *Proceedings of the Twelfth International Conference on Learning Representations*, 2024b. URL <https://openreview.net/forum?id=JePfAI8fah>.
- Liu, Y., Qin, G., Huang, X., Wang, J., and Long, M. Autotimes: Autoregressive time series forecasters via large language models. *arXiv preprint arXiv:2402.02370*, 2024c.
- Liu, Y., Qin, G., Huang, X., Wang, J., and Long, M. Autotimes: Autoregressive time series forecasters via large language models. *arXiv preprint arXiv:2402.02370*, 2024d.
- Ng, W. T., Siu, K., Cheung, A. C., and Ng, M. K. Expressing multivariate time series as graphs with time series attention transformer. *arXiv preprint arXiv:2208.09300*, 2022. URL <https://arxiv.org/abs/2208.09300>.
- Nie, Y., Nguyen, N. H., Sinthong, P., and Kalagnanam, J. A time series is worth 64 words: Long-term forecasting with transformers. In *Proceedings of the Eleventh International Conference on Learning Representations*, 2023. URL <https://openreview.net/forum?id=Jbdc0vTOcol>.
- Oreshkin, B. N., Carpol, D., Chapados, N., and Bengio, Y. N-beats: Neural basis expansion analysis for interpretable time series forecasting. In *International Conference on Learning Representations*, 2020. URL <https://openreview.net/forum?id=r1ecqn4YwB>.
- Park, D. S., Chan, W., Zhang, Y., Chiu, C.-C., Zoph, B., Cubuk, E. D., and Le, Q. V. SpecAugment: A simple data augmentation method for automatic speech recognition. *arXiv preprint arXiv:1904.08779*, 2019.

- Piao, X., Chen, Z., Murayama, T., Matsubara, Y., and Sakurai, Y. Fredformer: Frequency debiased transformer for time series forecasting. In *Proceedings of the 30th ACM SIGKDD Conference on Knowledge Discovery and Data Mining*, KDD '24, 2024.
- Rahaman, N., Baratin, A., Arpit, D., Draxler, F., Lin, M., Hamprecht, F., Bengio, Y., and Courville, A. On the spectral bias of neural networks. In *International conference on machine learning*, pp. 5301–5310. PMLR, 2019.
- Ryu, H., Yoon, S., Yoon, H. S., Yoon, E., and Yoo, C. D. Simpsi: A simple strategy to preserve spectral information in time series data augmentation. In *Proceedings of the AAAI Conference on Artificial Intelligence*, volume 38, pp. 14857–14865, 2024.
- Shang, Z., Chen, L., Wu, B., and Cui, D. Ada-mshyper: Adaptive multi-scale hypergraph transformer for time series forecasting. In *The Thirty-eighth Annual Conference on Neural Information Processing Systems*, 2024.
- Stock, J. H. and Watson, M. W. Forecasting using principal components from a large number of predictors. *Journal of the American statistical association*, 97(460):1167–1179, 2002.
- Sundararajan, R. R. and Bruce, S. A. Frequency band analysis of nonstationary multivariate time series. *arXiv preprint arXiv:2301.03664*, 2023.
- Tishby, N. and Zaslavsky, N. Deep learning and the information bottleneck principle. In *2015 IEEE Information Theory Workshop (ITW)*, Apr 2015. doi: 10.1109/itw.2015.7133169. URL <http://dx.doi.org/10.1109/itw.2015.7133169>.
- Toner, W. and Darlow, L. N. An analysis of linear time series forecasting models. In *Proceedings of the Forty-first International Conference on Machine Learning (ICML)*, 2024. URL <https://openreview.net/forum?id=x182CcbYaT>.
- Torres, J. F., Hadjout, D., Sebaa, A., Martínez-Alvarez, F., and Troncoso, A. Deep learning for time series forecasting: a survey. *Big Data*, 9(1):3–21, 2021.
- Wang, H., Peng, J., Huang, F., Wang, J., Chen, J., and Xiao, Y. MICN: Multi-scale local and global context modeling for long-term series forecasting. In *The Eleventh International Conference on Learning Representations*, 2023. URL <https://openreview.net/forum?id=zt53IDUR1U>.
- Wang, S., Wu, H., Shi, X., Hu, T., Luo, H., Ma, L., Zhang, J. Y., and ZHOU, J. Timemixer: Decomposable multi-scale mixing for time series forecasting. In *International Conference on Learning Representations (ICLR)*, 2024a.
- Wang, X., Zhou, T., Wen, Q., Gao, J., Ding, B., and Jin, R. CARD: Channel aligned robust blend transformer for time series forecasting. In *The Twelfth International Conference on Learning Representations*, 2024b. URL <https://openreview.net/forum?id=MJksrOhurE>.
- Wang, Y., Wu, H., Dong, J., Liu, Y., Long, M., and Wang, J. Deep time series models: A comprehensive survey and benchmark. *arXiv preprint arXiv:2407.13278*, 2024c. URL <https://arxiv.org/abs/2407.13278>.
- Wang, Z., Kong, F., Feng, S., Wang, M., Zhao, H., Wang, D., and Zhang, Y. Is mamba effective for time series forecasting? *arXiv preprint arXiv:2403.11144*, 2024d.
- Wen, Q., Zhou, T., Zhang, C., Chen, W., Ma, Z., Yan, J., and Sun, L. Transformers in time series: A survey. *arXiv preprint arXiv:2202.07125*, 2022.
- Wu, H., Xu, J., Wang, J., and Long, M. Autoformer: Decomposition transformers with auto-correlation for long-term series forecasting. In Ranzato, M., Beygelzimer, A., Dauphin, Y., Liang, P., and Vaughan, J. W. (eds.), *Advances in Neural Information Processing Systems*, volume 34, pp. 22419–22430. Curran Associates, Inc., 2021. URL https://proceedings.neurips.cc/paper_files/paper/2021/file/bcc0d400288793e8bcd7c19a8ac0c2b-Paper.pdf.
- Wu, H., Hu, T., Liu, Y., Zhou, H., Wang, J., and Long, M. TimesNet: Temporal 2d-variation modeling for general time series analysis. In *The Eleventh International Conference on Learning Representations*, 2023. URL https://openreview.net/forum?id=ju_Uqw3840q.
- Xu, Z., Zeng, A., and Xu, Q. Fits: Modeling time series with 10k parameters. In *Proceedings of the Twelfth International Conference on Learning Representations*, 2024a. URL <https://openreview.net/forum?id=bWcnvZ3qMb>.
- Xu, Z.-Q. J., Zhang, Y., and Luo, T. Overview frequency principle/spectral bias in deep learning. *Communications on Applied Mathematics and Computation*, pp. 1–38, 2024b.
- Yi, K., Zhang, Q., Cao, L., Wang, S., Long, G., Hu, L., He, H., Niu, Z., Fan, W., and Xiong, H. A survey on deep learning based time series analysis with frequency transformation. *arXiv preprint arXiv:2302.02173*, 2023a.
- Yi, K., Zhang, Q., Fan, W., He, H., Hu, L., Wang, P., An, N., Cao, L., and Niu, Z. FourierGNN: Rethinking multivariate time series forecasting from a pure graph perspective. In *Thirty-seventh Conference on Neural In-*

- formation Processing Systems, 2023b. URL <https://openreview.net/forum?id=bGslqWQ1Fx>.
- Yi, K., Zhang, Q., Fan, W., Wang, S., Wang, P., He, H., An, N., Lian, D., Cao, L., and Niu, Z. Frequency-domain MLPs are more effective learners in time series forecasting. In *Thirty-seventh Conference on Neural Information Processing Systems*, 2023c. URL <https://openreview.net/forum?id=iif9mGCTfy>.
- Yi, K., Fei, J., Zhang, Q., He, H., Hao, S., Lian, D., and Fan, W. Filternet: Harnessing frequency filters for time series forecasting. *arXiv preprint arXiv:2411.01623*, 2024.
- Yu, C., Wang, F., Shao, Z., Sun, T., Wu, L., and Xu, Y. Dsformer: A double sampling transformer for multivariate time series long-term prediction. In *Proceedings of the 32nd ACM international conference on information and knowledge management*, pp. 3062–3072, 2023.
- Yu, G., Li, Y., Guo, X., Wang, D., Liu, Z., Wang, S., and Yang, T. Lino: Advancing recursive residual decomposition of linear and nonlinear patterns for robust time series forecasting. *arXiv preprint arXiv:2410.17159*, 2024a.
- Yu, G., Zou, J., Hu, X., Aviles-Rivero, A. I., Qin, J., and Wang, S. Revitalizing multivariate time series forecasting: Learnable decomposition with inter-series dependencies and intra-series variations modeling. In *Proceedings of the Forty-first International Conference on Machine Learning (ICML)*, 2024b. URL <https://openreview.net/forum?id=87CYNyCG0o>.
- Zeng, A., Chen, M., Zhang, L., and Xu, Q. Are transformers effective for time series forecasting? In *Proceedings of the AAAI Conference on Artificial Intelligence*, volume 37, pp. 11121–11128, 2023. URL <https://ojs.aaai.org/index.php/AAAI/article/view/26317/26089>.
- Zhang, T., Zhang, Y., Cao, W., Bian, J., Yi, X., Zheng, S., and Li, J. Less is more: Fast multivariate time series forecasting with light sampling-oriented mlp structures. *arXiv preprint arXiv:2207.01186*, 2022. URL <https://arxiv.org/abs/2207.01186>.
- Zhang, Y. and Yan, J. Crossformer: Transformer utilizing cross-dimension dependency for multivariate time series forecasting. In *The Eleventh International Conference on Learning Representations*, 2023. URL <https://openreview.net/forum?id=vSVLM2j9eie>.
- Zhao, L. and Shen, Y. Rethinking channel dependence for multivariate time series forecasting: Learning from leading indicators. In *The Twelfth International Conference on Learning Representations*, 2024. URL <https://openreview.net/forum?id=JiTVtCUOpS>.
- Zhou, H., Zhang, S., Peng, J., Zhang, S., Li, J., Xiong, H., and Zhang, W. Informer: Beyond efficient transformer for long sequence time-series forecasting. *Proceedings of the AAAI Conference on Artificial Intelligence*, 35:11106–11115, 2022a. doi: 10.1609/aaai.v35i12.17325. URL <http://dx.doi.org/10.1609/aaai.v35i12.17325>.
- Zhou, T., MA, Z., wang, x., Wen, Q., Sun, L., Yao, T., Yin, W., and Jin, R. Film: Frequency improved legendre memory model for long-term time series forecasting. In Koyejo, S., Mohamed, S., Agarwal, A., Belgrave, D., Cho, K., and Oh, A. (eds.), *Advances in Neural Information Processing Systems*, volume 35, pp. 12677–12690. Curran Associates, Inc., 2022b.
- Zhou, T., Ma, Z., Wen, Q., Wang, X., Sun, L., and Jin, R. Fedformer: Frequency enhanced decomposed transformer for long-term series forecasting. In *Proceedings of the 39th International Conference on Machine Learning (ICML 2022)*, 2022c.
- Zhou, Y., You, L., Zhu, W., and Xu, P. Improving time series forecasting with mixup data augmentation. 2023.

A. Proof

This section is dedicated to proving Theorem 3.3 and Theorem 3.5.

A.1. Impact of RevIN on Frequency Spectrum

RevIN (Kim et al., 2022; Liu et al., 2022c) normalizes inputs using sample-wise mean and variance, then reverts scaling post-prediction to ensure consistent distributions, mitigating non-stationary effects in time series.

Let the original time series be $x(t)$ with length T . The series $\hat{x}(t)$ that processed by RevIN is given by:

$$\begin{aligned}\hat{x}(t) &= \frac{x(t) - \mu}{\sigma}, t = 0, 1, \dots, T - 1, \\ \mu &= \frac{1}{T} \sum_{t=0}^{T-1} x(t), \quad \sigma = \sqrt{\frac{1}{T} \sum_{t=0}^{T-1} (x(t) - \mu)^2}.\end{aligned}\quad (8)$$

The Fourier transform of $x(t)$ and $\hat{x}(t)$ are:

$$\begin{aligned}X(f) &= \sum_{t=0}^{T-1} x(t) e^{-i2\pi f t / T - 1}, \quad f = 0, 1, \dots, T - 1, \\ \hat{X}(f) &= \sum_{t=0}^{T-1} \left(\frac{x(t) - \mu}{\sigma} \right) e^{-i2\pi f t / T - 1} \\ &= \frac{1}{\sigma} \sum_{t=0}^{T-1} x(t) e^{-i2\pi f t / T - 1} - \frac{\mu}{\sigma} \sum_{t=0}^{T-1} e^{-i2\pi f t / T - 1}.\end{aligned}\quad (9)$$

The spectral energy is computed as the squared magnitude of the Fourier transform. For $x(t)$ and $\hat{x}(t)$, we have:

$$E_X(f) = |X(f)|^2, \quad E_{\hat{X}}(f) = |\hat{X}(f)|^2. \quad (10)$$

When $f = 0$, the exponential term $e^{-i2\pi f t / T - 1} = 1$, so:

$$\begin{aligned}\hat{X}(0) &= \frac{1}{\sigma} \sum_{t=0}^{T-1} x(t) - \frac{\mu T}{\sigma} \\ &= \frac{\mu T}{\sigma} - \frac{\mu T}{\sigma} \\ &= 0\end{aligned}\quad (11)$$

Since $\frac{\mu}{\sigma}$ is a constant, we have:

$$\begin{aligned}\frac{\mu}{\sigma} \cdot \sum_{t=0}^{T-1} e^{-i2\pi f t / T - 1} &= 0, \quad f = 1, 2, \dots, T - 1, \\ \hat{X}(f) &= \frac{1}{\sigma} \sum_{t=0}^{T-1} x(t) e^{-i2\pi f t / T - 1} - \frac{\mu}{\sigma} \sum_{t=0}^{T-1} e^{-i2\pi f t / T - 1} \\ &= \frac{1}{\sigma} X(f), \\ E_{\hat{X}}(f) &= \left(\frac{1}{\sigma} \right)^2 |X(f)|^2.\end{aligned}\quad (12)$$

This suggests that RevIN scales the spectral energy by σ^2 but does not affect its relative distribution except $\hat{X}(0) = 0$. Thus, RevIN preserves the relative spectral energy distribution and leaves the Mid-Frequency Spectrum Gap unresolved.

A.2. Impact of AMEO on Frequency Spectrum

Referring back to Definition 3.4, AMEO is defined as:

$$\begin{aligned}\hat{x}(t) &= x(t) - \frac{\beta}{K} \sum_{k=0}^{K-1} \tilde{x}(t + K - 1 - k), \\ \tilde{x}(t) &= \begin{cases} x(t - (\frac{K}{2} + 1)), & \text{if } \frac{K}{2} + 1 \leq t < T + \frac{K}{2} + 1 \\ 0, & \text{if } 0 \leq t < \frac{K}{2} + 1 \text{ or } T + \frac{K}{2} + 1 \leq t < T + K \end{cases}\end{aligned}\quad (13)$$

The Fourier transform of $\hat{x}(t)$ is:

$$\begin{aligned}\hat{X}(f) &= \sum_{t=0}^{T-1} \left[x(t) - \frac{\beta}{K} \sum_{k=0}^{K-1} \tilde{x}(t + K - 1 - k) \right] e^{-i2\pi f t / T - 1} \\ &= \underbrace{\sum_{t=0}^{T-1} x(t) e^{-i2\pi f t / T - 1}}_{X(f)} - \frac{\beta}{K} \sum_{k=0}^{K-1} \underbrace{\sum_{t=0}^{T-1} \tilde{x}(t + K - 1 - k) e^{-i2\pi f t / T - 1}}_{T_k(f)}.\end{aligned}\quad (14)$$

For $T_k(f)$, given $FFT\{x(t - a)\} = X(f) e^{-i2\pi f a / T - 1}$, we have:

$$\begin{aligned}T_k(f) &= \sum_{t=0}^{T-1} \tilde{x}(t + K - 1 - k) e^{-i2\pi f t / T - 1} \\ &= \sum_{t=0}^{T-1} x(t + \frac{3K}{2} - k - 2) e^{-i2\pi f t / T - 1} \\ &= FFT\{x(t + \frac{3K}{2} - k - 2)\} \\ &= X(f) e^{i2\pi f (\frac{3K}{2} - k - 2) / T - 1}\end{aligned}\quad (15)$$

So, we have the Fourier transform of $\hat{x}(t)$ and its spectral energy:

$$\begin{aligned}\hat{X}(f) &= X(f) - \frac{\beta}{K} \sum_{k=0}^{K-1} X(f) e^{i2\pi f(\frac{3K}{2}-k-2)/T-1} \\ &= X(f) \left[1 - \beta \cdot \underbrace{\frac{1}{K} \sum_{k=0}^{K-1} e^{i2\pi f(\frac{3K}{2}-k-2)/T-1}}_{G(f)} \right], \\ E_{\hat{X}}(f) &= |X(f)|^2 \left\{ 1 - \beta \cdot \underbrace{\frac{1}{K} \sum_{k=0}^{K-1} e^{i2\pi f(\frac{3K}{2}-k-2)/T-1}}_{G(f)} \right\}^2 \\ &= |X(f)|^2 (1 - \beta \cdot G(f))^2. \quad (16)\end{aligned}$$

In this paper, we set $K = 25$ (i.e., $T/4 + 1$, $T = 96$), and the function graph of $G(f)$ is shown in Figure 6.

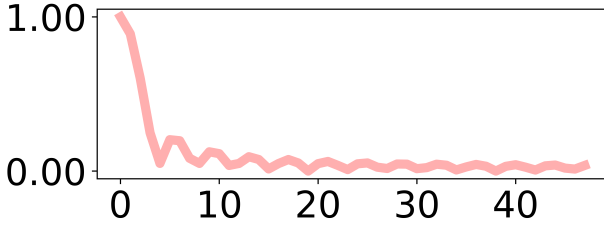


Figure 6: The function $G(f)$ is plotted for $T = 96$ and $K = 25$. Due to the symmetry of the FFT , we only need to plot the values for $f = 0, 1, \dots, 48$.

It is evident that $G(f)$ is a gradually decay function, with its values decreasing **from 1 to 0**. This ensures that $E_{\hat{X}}(f) = |X(f)|^2 (1 - \beta \cdot G(f))^2$, where, relative to E_X , the low-frequency components are attenuated, and the mid-frequency components are enhanced.

B. EXPERIMENTAL DETAILS

B.1. Dataset Statistics

We elaborate on the datasets employed in this study with the following details.

- **ETT Dataset** (Zhou et al., 2022a) comprises two sub-datasets: **ETTh** and **ETTm**, which were collected from electricity transformers. Data were recorded at 15-minute and 1-hour intervals for ETTm and ETTh, respectively, spanning from July 2016 to July 2018.
- **Solar Energy** (Lai et al., 2018) records the solar power

production of 137 PV plants in 2006, which are sampled every 10 minutes.

- **Electricity Dataset**² encompasses the electricity consumption data of 321 customers, recorded on an hourly basis, covering the period from 2012 to 2014.
- **Traffic Dataset**³ consists of hourly data from the California Department of Transportation. It describes road occupancy rates measured by various sensors on San Francisco Bay area freeways.
- **Weather Dataset**⁴ contains records of 21 meteorological indicators, updated every 10 minutes throughout the entire year of 2020.

We follow the same data processing and train-validation-test set split protocol used in iTransformer (Liu et al., 2024b), where the train, validation, and test datasets are strictly divided according to chronological order to make sure there are no data leakage issues. We fix the input length as $T = 96$ for all datasets, and the forecasting length $F \in \{96, 192, 336, 720\}$.

B.2. Implementation Details and Model Parameters

We trained our ReFocus model using the MSE loss function and employed the ADAM optimizer. For evaluation purposes, we used two key performance metrics: the mean square error (MSE) and the mean absolute error (MAE). We initialized the random seed as $rs = 2024$ and set the hyper-parameter $K = 25$ -kernel size of the convolution kernel in AMEO. The dimension of the Layer is set to $D = 512$ and $Q = 128$. The batch size $bs = 32$ for the Traffic dataset due to its large channel will cause **out of memory** when employed with large batch size, and $bs = 128$ for others. The learning rate is searched from $lr \in \{1e-5, 1e-4\}$ except for the Traffic dataset ($lr = 5e-4$). The number of EKPB is searched from $N \in \{1, 2, 3, 4\}$, and hyper-parameter β , which controls the scale magnitude, from $\beta \in \{0.01, 0.1, 0.5, 1.0\}$. Our implementation was carried out in PyTorch and executed on a single NVIDIA GeForce RTX 4090 with 24G VRAM. To foster reproducibility, we make our code, and training scripts available in this **GitHub Repository**⁵.

All the compared multivariate forecasting baseline models that we reproduced are implemented based on the benchmark of **Time series Lab** (Wang et al., 2024c) Repository⁶,

²<https://archive.ics.uci.edu/ml/datasets/ElectricityLoadDiagrams20112014>

³<https://pems.dot.ca.gov/>

⁴<https://www.bgc-jena.mpg.de/wetter/>

⁵<https://github.com/Levi-Ackman/ReFocus>

⁶<https://github.com/thuml/Time-Series-Library>

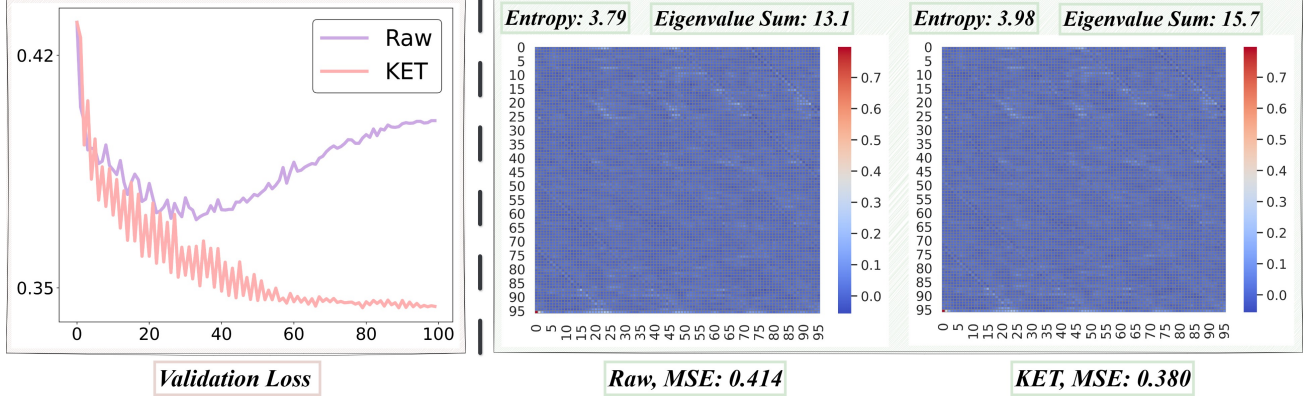


Figure 7: We select the *input* – 96 – *forecast* – 96 task on Traffic and visualize the validation loss and weight of our **ReFocus** model. **LEFT:** Visualization of the **Validation Loss** during 100 training epochs with (**KET**) and without **KET** (**Raw**). **RIGHT:** Visualization about the Weight (Obtained using the approach outlined in **Analysis of linear model** (Toner & Darlow, 2024)) of the trained model. Two significant metrics for assessing the information richness of the weight matrix—the information **Entropy** and the **Sum of Eigenvalues**—are calculated. Both indicate higher quality with greater values.

which is fairly built on the configurations provided by each model’s original paper or official code. Those that have not yet been included in **Time series Lab** are directly reproduced from their official code repositories. It is worth noting that both the baselines used in this paper and our **ReFocus** have fixed a long-standing bug. This bug was originally identified in Informer (Zhou et al., 2022a) (AAAI 2021 Best Paper) and subsequently addressed by FITS (Xu et al., 2024a). For specific details about the bug and its resolution, please refer to **GitHub Repository**⁷.

C. Further Analysis of the proposed Key-Frequency Enhanced Training strategy

To further investigate the impact of the proposed ‘**Key-Frequency Enhanced Training (KET) strategy**’ on model training and forecasting ability, we visualize its training process regarding Validation Loss and the model weights obtained after training in Figure 7. We also compute the **Entropy** and the **Sum of Eigenvalues** of the weight matrix.

The results show that, in the absence of KET, the model quickly overfits around the **24**th epoch, exhibiting poor generalization. In contrast, with the aid of KET, the model consistently performs better on the validation set, converging smoothly without overfitting, and the training process becomes more stable. Additionally, weight visualization results indicate that the model trained with KET has higher information **Entropy** and a greater **Sum of Eigenvalues**, suggesting that the trained model possesses a stronger capacity for feature representation extraction. The predictive results further validate this, as our KET improves the MSE from 0.414 to 0.380, achieving an **8.2%** reduction.

⁷<https://github.com/VEWOXIC/FITS>

D. Full Results

The full experiment results are provided in the following section due to the space limitation of the main text.

Full multivariate forecasting results Table 9 contains the detailed results of Ten baselines and our ReFocus on eight well-acknowledged forecasting benchmarks. ReFocus consistently achieves the best overall performance across all datasets, especially in tasks with a large number of channels, such as the Solar_Energy dataset (137 channels), ECL dataset (321 channels), and Traffic dataset (862 channels). It obtains the best performance in terms of MSE: **35 out of 40** tasks, and MAE: **38 out of 40** tasks. These results demonstrate the outstanding performance of ReFocus in multivariate time series forecasting tasks.

Full results of ablation on AMEO and KET Table D presents the full results of the ablation study on ‘Adaptive Mid-Frequency Energy Optimizer (AMEO)’ and ‘Key-Frequency Enhanced Training (KET)’. KET and AMEO contribute significantly to the model’s performance, each providing substantial improvements. Moreover, their combination further enhances the model, achieving peak performance. These results provide strong evidence of the effectiveness of both AMEO and KET.

Full results of further ablation study on KET Table D exhibits the full results of a further ablation study on the ‘Key-Frequency Enhanced Training (KET)’ strategy. Introducing Pseudo samples—obtained by randomly incorporating spectral information from other channels into the current channel—generally leads to performance improvement. However, on more complex datasets, it results in performance degradation. In contrast, alternating training between Real and Pseudo samples (**Our KET**) overcomes

this issue, yielding a further and consistent enhancement in performance.

Full results of ablation study of different Key-Frequency

Picking strategies Table D illustrates the complete results of the ablation study on various Key-Frequency Picking strategies. Notably, our **Softmax-based random sampling** strategy consistently achieves the best overall performance, particularly on more complex datasets.

Full results of EKPB and other inter-series dependencies

modeling backbone Table D presents the full results of ‘Energy-based Key-Frequency Picking Block (EKPB)’ and other inter-series dependency modeling backbones on multivariate time series forecasting tasks. The proposed EKPB achieves overall optimal performance, demonstrating exceptional capability in modeling inter-series dependencies.

Table 9: Multivariate long-term forecasting result comparison. We use prediction lengths $F \in \{96, 192, 336, 720\}$, and input length $T = 96$. The best results are in **bold** and the second bests are underlined.

Model	ReFocus (Ours)	FilterNet (2024)	iTransformer (2024b)	ModernTCN (2024)	FITS (2024a)	PatchTST (2023)	Crossformer (2023)	TimesNet (2023)	TSMixer (2023)	DLinear (2023)	FreTS (2023c)	
Metric	MSE	MAE	MSE	MAE	MSE	MAE	MSE	MAE	MSE	MAE	MSE	MAE
ETTm1	96	0.321 0.360	<u>0.321</u> <u>0.361</u>	0.334 0.368	0.317 0.362	0.355 0.375	0.329 0.367	0.404 0.426	0.338 0.375	0.323 0.363	0.345 0.372	0.335 0.372
	192	0.365 0.379	0.367 0.387	0.377 0.391	0.366 0.389	0.392 0.393	<u>0.367</u> <u>0.385</u>	0.450 0.451	0.374 0.387	0.376 0.392	0.380 0.389	0.388 0.401
	336	0.398 0.400	0.401 0.409	0.426 0.420	0.407 0.412	0.424 0.414	<u>0.399</u> <u>0.410</u>	0.532 0.515	0.410 0.411	0.407 0.413	0.413 0.413	0.421 0.426
	720	0.463 0.437	0.477 0.448	0.491 0.459	0.466 0.443	0.487 0.449	<u>0.454</u> <u>0.439</u>	0.666 0.589	0.478 0.450	0.485 0.459	0.474 0.453	0.486 0.465
	Avg	0.387 0.394	0.392 0.401	0.407 0.410	0.389 0.402	0.415 0.408	<u>0.387</u> <u>0.400</u>	0.513 0.496	0.400 0.406	0.398 0.407	0.403 0.407	0.408 0.416
ETTm2	96	0.173 0.255	0.175 0.258	0.180 0.264	<u>0.173</u> <u>0.255</u>	0.183 0.266	0.175 0.259	0.287 0.366	0.187 0.267	0.182 0.266	0.193 0.292	0.189 0.277
	192	0.237 0.297	0.240 0.301	0.250 0.309	0.235 0.296	0.247 0.305	0.241 0.302	0.414 0.492	0.249 0.309	0.249 0.309	0.284 0.362	0.258 0.326
	336	0.295 0.334	0.311 0.347	0.311 0.348	0.308 0.344	0.307 <u>0.342</u>	<u>0.305</u> 0.343	0.597 0.542	0.321 0.351	0.309 0.347	0.369 0.427	0.343 0.390
	720	0.395 0.392	0.414 0.405	0.412 0.407	<u>0.398</u> <u>0.394</u>	0.407 0.399	0.402 0.400	1.730 1.042	0.408 0.403	0.416 0.408	0.554 0.522	0.495 0.480
	Avg	0.275 0.320	0.285 0.328	0.288 0.332	<u>0.279</u> <u>0.322</u>	0.286 0.328	0.281 0.326	0.757 0.610	0.291 0.333	0.289 0.333	0.350 0.401	0.321 0.368
ETTh1	96	0.376 0.394	<u>0.382</u> 0.402	0.386 0.405	0.386 <u>0.394</u>	0.386 0.396	0.414 0.419	0.423 0.448	0.384 0.402	0.401 0.412	0.386 0.400	0.395 0.407
	192	0.428 0.422	<u>0.430</u> 0.429	0.441 0.436	0.436 0.423	0.436 <u>0.423</u>	0.460 0.445	0.471 0.474	0.436 0.429	0.452 0.442	0.437 0.432	0.448 0.440
	336	0.462 0.442	<u>0.472</u> 0.451	0.487 0.458	0.479 <u>0.445</u>	0.478 0.444	0.501 0.466	0.570 0.546	0.491 0.469	0.492 0.463	0.481 0.459	0.499 0.472
	720	0.470 0.474	<u>0.481</u> 0.473	0.503 0.491	0.481 <u>0.469</u>	0.502 0.495	0.500 0.488	0.653 0.621	0.521 0.500	0.507 0.490	0.519 0.516	0.558 0.532
	Avg	0.434 0.433	<u>0.441</u> 0.439	0.454 0.447	0.446 <u>0.433</u>	0.451 0.440	0.469 0.454	0.529 0.522	0.458 0.450	0.463 0.452	0.456 0.452	0.475 0.463
ETTh2	96	0.288 0.337	0.293 0.343	0.297 0.349	<u>0.292</u> <u>0.340</u>	0.295 0.350	0.302 0.348	0.745 0.584	0.340 0.374	0.319 0.361	0.333 0.387	0.309 0.364
	192	0.371 0.390	0.374 0.396	0.380 0.400	<u>0.377</u> <u>0.395</u>	0.381 0.396	0.388 0.400	0.877 0.656	0.402 0.414	0.402 0.410	0.477 0.476	0.395 0.425
	336	0.409 0.421	0.417 0.430	0.428 0.432	<u>0.424</u> <u>0.434</u>	0.426 0.438	0.426 0.433	1.043 0.731	0.452 0.452	0.444 0.446	0.594 0.541	0.462 0.467
	720	0.417 0.436	0.449 0.460	0.427 0.445	<u>0.433</u> <u>0.448</u>	0.431 0.446	0.431 0.446	1.104 0.763	0.462 0.468	0.441 0.450	0.831 0.657	0.721 0.604
	Avg	0.371 0.396	0.383 0.407	0.383 0.407	<u>0.382</u> <u>0.404</u>	0.383 0.408	0.387 0.407	0.942 0.684	0.414 0.427	0.401 0.417	0.559 0.515	0.472 0.465
ECL	96	0.143 0.238	<u>0.147</u> 0.245	0.148 <u>0.240</u>	0.173 0.260	0.200 0.278	0.181 0.270	0.219 0.314	0.168 0.272	0.157 0.260	0.197 0.282	0.176 0.258
	192	0.158 0.252	<u>0.160</u> 0.250	0.162 0.253	0.181 0.267	0.200 0.280	0.188 0.274	0.231 0.322	0.184 0.289	0.173 0.274	0.196 0.285	0.175 0.262
	336	0.172 0.267	<u>0.173</u> 0.267	0.178 0.269	0.196 0.283	0.214 0.295	0.204 0.293	0.246 0.337	0.198 0.300	0.192 0.295	0.209 0.301	0.185 0.278
	720	0.198 0.290	<u>0.210</u> 0.309	0.225 0.317	0.238 0.316	0.255 0.327	0.246 0.324	0.280 0.363	0.220 0.320	0.223 0.318	0.245 0.333	0.220 0.315
	Avg	0.168 0.262	<u>0.173</u> 0.268	0.178 0.270	0.197 0.282	0.217 0.295	0.205 0.290	0.244 0.334	0.192 0.295	0.186 0.287	0.212 0.300	0.189 0.278
Traffic	96	0.380 0.248	0.430 0.294	<u>0.395</u> 0.268	0.550 0.355	0.651 0.391	0.462 0.295	0.522 0.290	0.593 0.321	0.493 0.336	0.650 0.396	0.593 0.378
	192	0.403 0.259	0.452 0.307	<u>0.417</u> 0.276	0.527 0.337	0.602 0.363	0.466 0.296	0.530 0.293	0.617 0.336	0.497 0.351	0.598 0.370	0.595 0.377
	336	0.419 0.267	0.470 0.316	<u>0.433</u> 0.283	0.537 0.342	0.609 0.366	0.482 0.304	0.558 0.305	0.629 0.336	0.528 0.361	0.605 0.373	0.609 0.385
	720	0.446 0.287	0.498 0.323	<u>0.467</u> 0.302	0.570 0.359	0.647 0.385	0.514 0.322	0.589 0.328	0.640 0.350	0.569 0.380	0.645 0.394	0.673 0.418
	Avg	0.412 0.265	0.463 0.310	<u>0.428</u> 0.282	0.546 0.348	0.627 0.376	0.481 0.304	0.550 0.304	0.620 0.336	0.522 0.357	0.625 0.383	0.618 0.390
Weather	96	0.160 0.202	0.162 <u>0.207</u>	0.174 0.214	0.165 0.203	0.166 0.213	0.177 0.218	0.158 0.230	0.172 0.220	0.166 0.210	0.196 0.255	0.174 0.208
	192	0.211 0.248	<u>0.210</u> 0.250	0.221 0.254	0.212 0.247	0.213 0.254	0.225 0.259	0.206 0.277	0.219 0.261	0.215 0.256	0.237 0.296	0.219 0.250
	336	0.266 0.290	0.265 0.290	0.278 0.296	0.266 0.293	0.269 0.294	0.278 0.297	0.272 0.335	0.280 0.306	0.287 0.300	0.283 0.335	0.273 0.290
	720	0.344 0.343	0.342 0.340	0.358 0.349	0.344 0.343	0.346 0.343	0.354 0.348	0.398 0.418	0.365 0.359	0.355 0.348	0.345 0.381	0.334 0.332
	Avg	0.245 0.271	<u>0.245</u> 0.272	0.258 0.279	0.247 0.272	0.249 0.276	0.259 0.281	0.259 0.315	0.259 0.287	0.256 0.279	0.265 0.317	0.250 0.270
Solar_Energy	96	0.182 0.219	0.206 0.251	<u>0.203</u> 0.237	0.206 0.264	0.371 0.417	0.234 0.286	0.310 0.331	0.250 0.292	0.221 0.275	0.290 0.378	0.217 0.278
	192	0.222 0.249	0.242 0.279	<u>0.233</u> 0.261	0.246 0.285	0.377 0.398	0.267 0.310	0.734 0.725	0.296 0.318	0.268 0.306	0.320 0.398	0.256 0.302
	336	0.240 0.268	0.255 0.291	<u>0.248</u> 0.273	0.260 0.296	0.416 0.412	0.290 0.315	0.750 0.735	0.319 0.330	0.272 0.294	0.353 0.415	0.263 0.307
	720	0.242 0.271	0.267 0.301	<u>0.249</u> 0.275	0.264 0.298	0.414 0.400	0.289 0.317	0.769 0.765	0.338 0.337	0.281 0.313	0.356 0.413	0.256 0.297
	Avg	0.222 0.252	0.243 0.283	<u>0.233</u> 0.262	0.244 0.286	0.395 0.407	0.270 0.307	0.641 0.639	0.301 0.319	0.260 0.297	0.330 0.401	0.248 0.296
1 st Count		34	38	2	1	0	0	1	1	0	0	0
								0	0	1	0	0
								2	0	0	0	0
								0	0	0	0	0
								0	0	0	0	0

Table 10: Full result of ablation study on the ‘Adaptive Mid-Frequency Energy Optimizer (AMEO)’ and the ‘Key-Frequency Enhanced Training (KET)’ strategy. We use prediction lengths $F \in \{96, 192, 336, 720\}$, and input length $T = 96$. The best results are in **bold**.

Model	Both (ReFocus)	+ AMEO		+ KET		None	
		MSE	MAE	MSE	MAE	MSE	MAE
ETTm1	96	0.321	0.360	0.331	0.368	0.331	0.363
	192	0.365	0.379	0.377	0.390	0.373	0.382
	336	0.398	0.400	0.403	0.407	0.403	0.402
	720	0.463	0.437	0.462	0.441	0.467	0.438
	Avg	0.387	0.394	0.393	0.402	0.394	0.396
ETTm2	96	0.173	0.255	0.179	0.262	0.178	0.260
	192	0.237	0.297	0.244	0.304	0.241	0.299
	336	0.295	0.334	0.304	0.340	0.300	0.337
	720	0.395	0.392	0.402	0.396	0.398	0.393
	Avg	0.275	0.320	0.282	0.326	0.279	0.322
ETTh1	96	0.376	0.394	0.382	0.398	0.378	0.395
	192	0.428	0.422	0.433	0.425	0.432	0.423
	336	0.462	0.442	0.468	0.450	0.469	0.447
	720	0.470	0.474	0.489	0.486	0.470	0.474
	Avg	0.434	0.433	0.443	0.440	0.437	0.435
ETTh2	96	0.288	0.337	0.285	0.336	0.289	0.339
	192	0.371	0.390	0.375	0.391	0.374	0.390
	336	0.409	0.421	0.405	0.420	0.412	0.425
	720	0.417	0.436	0.424	0.441	0.418	0.438
	Avg	0.371	0.396	0.372	0.397	0.373	0.398
ECL	96	0.143	0.238	0.146	0.241	0.145	0.239
	192	0.158	0.252	0.165	0.259	0.161	0.253
	336	0.172	0.267	0.177	0.272	0.176	0.269
	720	0.198	0.290	0.206	0.297	0.203	0.292
	Avg	0.168	0.262	0.174	0.267	0.171	0.263
Traffic	96	0.380	0.248	0.414	0.274	0.380	0.250
	192	0.403	0.259	0.439	0.287	0.404	0.262
	336	0.419	0.267	0.449	0.288	0.421	0.270
	720	0.446	0.287	0.506	0.307	0.450	0.290
	Avg	0.412	0.265	0.452	0.289	0.414	0.268
Weather	96	0.160	0.202	0.165	0.209	0.164	0.207
	192	0.211	0.248	0.210	0.252	0.215	0.252
	336	0.266	0.290	0.267	0.291	0.273	0.295
	720	0.344	0.343	0.350	0.346	0.349	0.345
	Avg	0.245	0.271	0.248	0.275	0.250	0.275
Solar_Energy	96	0.182	0.219	0.197	0.226	0.192	0.230
	192	0.222	0.249	0.236	0.269	0.231	0.255
	336	0.240	0.268	0.246	0.276	0.244	0.271
	720	0.242	0.271	0.245	0.274	0.245	0.274
	Avg	0.222	0.252	0.231	0.261	0.228	0.258

Table 11: Full result of further ablation study on the ‘Key-Frequency Enhanced Training (KET)’ strategy. We use prediction lengths $F \in \{96, 192, 336, 720\}$, and input length $T = 96$. The best results are in **bold**.

Model	Both (KET)	Pseudo		Real	
		MSE	MAE	MSE	MAE
ETTm1					
	96	0.331	0.363	0.331 0.362	0.339 0.367
	192	0.373	0.382	0.375 0.384	0.381 0.391
	336	0.403	0.402	0.406 0.405	0.414 0.413
	720	0.467	0.438	0.471 0.440	0.468 0.442
	Avg	0.394	0.396	0.396 0.398	0.401 0.403
ETTm2					
	96	0.178	0.260	0.178 0.260	0.180 0.262
	192	0.241	0.299	0.242 0.299	0.245 0.302
	336	0.300	0.337	0.301 0.339	0.304 0.340
	720	0.398	0.393	0.399 0.393	0.404 0.396
	Avg	0.279	0.322	0.280 0.323	0.283 0.325
ERTh1					
	96	0.378	0.395	0.382 0.394	0.383 0.395
	192	0.432	0.423	0.429 0.423	0.432 0.425
	336	0.469	0.447	0.467 0.445	0.469 0.449
	720	0.470	0.474	0.467 0.472	0.474 0.480
	Avg	0.437	0.435	0.436 0.434	0.440 0.437
ERTh2					
	96	0.289	0.339	0.288 0.338	0.288 0.338
	192	0.374	0.390	0.370 0.390	0.374 0.391
	336	0.412	0.425	0.412 0.423	0.419 0.428
	720	0.418	0.438	0.418 0.437	0.423 0.441
	Avg	0.373	0.398	0.372 0.397	0.376 0.400
ECL					
	96	0.145	0.239	0.147 0.241	0.147 0.242
	192	0.161	0.253	0.165 0.257	0.162 0.256
	336	0.176	0.269	0.179 0.271	0.180 0.274
	720	0.203	0.292	0.209 0.296	0.221 0.307
	Avg	0.171	0.263	0.175 0.266	0.178 0.270
Traffic					
	96	0.380	0.250	0.383 0.254	0.414 0.278
	192	0.404	0.262	0.406 0.265	0.437 0.284
	336	0.421	0.270	0.424 0.272	0.449 0.288
	720	0.450	0.290	0.454 0.293	0.495 0.307
	Avg	0.414	0.268	0.417 0.271	0.449 0.289
Weather					
	96	0.164	0.207	0.166 0.207	0.164 0.209
	192	0.215	0.252	0.216 0.255	0.216 0.256
	336	0.273	0.295	0.275 0.297	0.275 0.299
	720	0.349	0.345	0.352 0.346	0.353 0.347
	Avg	0.250	0.275	0.253 0.276	0.252 0.278
Solar_Energy					
	96	0.192	0.230	0.235 0.263	0.192 0.234
	192	0.231	0.255	0.290 0.303	0.235 0.265
	336	0.244	0.271	0.287 0.301	0.249 0.279
	720	0.245	0.274	0.296 0.308	0.250 0.278
	Avg	0.228	0.258	0.277 0.294	0.232 0.264

Table 12: Full result about ablation study of different Key-Frequency Picking strategies. We use prediction lengths $F \in \{96, 192, 336, 720\}$, and input length $T = 96$. The best results are in **bold**.

Model	Softmax		Max		Min		
	Metric	MSE	MAE	MSE	MAE	MSE	MAE
ETTm1	96	0.321	0.360	0.331	0.360	0.321	0.357
	192	0.365	0.379	0.370	0.380	0.366	0.377
	336	0.398	0.400	0.401	0.402	0.400	0.399
	720	0.463	0.437	0.467	0.438	0.464	0.436
	Avg	0.387	0.394	0.392	0.395	0.388	0.392
ETTm2	96	0.173	0.255	0.175	0.258	0.177	0.259
	192	0.237	0.297	0.240	0.300	0.242	0.300
	336	0.295	0.334	0.303	0.338	0.302	0.338
	720	0.395	0.392	0.396	0.392	0.398	0.394
	Avg	0.275	0.320	0.279	0.322	0.280	0.323
ERTh1	96	0.376	0.394	0.380	0.396	0.372	0.391
	192	0.428	0.422	0.430	0.423	0.426	0.423
	336	0.462	0.442	0.464	0.444	0.464	0.443
	720	0.470	0.474	0.473	0.478	0.467	0.472
	Avg	0.434	0.433	0.437	0.435	0.432	0.432
ETTh2	96	0.288	0.337	0.289	0.340	0.287	0.337
	192	0.371	0.390	0.373	0.391	0.366	0.388
	336	0.409	0.421	0.414	0.425	0.410	0.423
	720	0.417	0.436	0.418	0.437	0.419	0.437
	Avg	0.371	0.396	0.374	0.398	0.371	0.396
ECL	96	0.143	0.238	0.145	0.241	0.165	0.256
	192	0.158	0.252	0.162	0.256	0.176	0.267
	336	0.172	0.267	0.175	0.269	0.192	0.283
	720	0.198	0.290	0.204	0.293	0.242	0.318
	Avg	0.168	0.262	0.172	0.265	0.194	0.281
Traffic	96	0.380	0.248	0.389	0.253	0.504	0.341
	192	0.403	0.259	0.413	0.268	0.505	0.338
	336	0.419	0.267	0.427	0.276	0.521	0.351
	720	0.446	0.287	0.457	0.296	0.536	0.347
	Avg	0.412	0.265	0.422	0.273	0.517	0.344
Weather	96	0.160	0.202	0.166	0.207	0.164	0.205
	192	0.211	0.248	0.212	0.248	0.212	0.249
	336	0.266	0.290	0.268	0.291	0.269	0.290
	720	0.344	0.343	0.348	0.344	0.349	0.344
	Avg	0.245	0.271	0.249	0.273	0.249	0.272
Solar_Energy	96	0.182	0.219	0.189	0.228	0.208	0.247
	192	0.222	0.249	0.236	0.262	0.242	0.270
	336	0.240	0.268	0.245	0.273	0.256	0.283
	720	0.242	0.271	0.248	0.276	0.253	0.280
	Avg	0.222	0.252	0.230	0.260	0.240	0.270

Table 13: Multivariate forecasting result of ‘Energy-based Key-Frequency Picking Block’ (EKPB) and other inter-series dependencies modeling backbones. We use prediction lengths $F \in \{96, 192, 336, 720\}$, and input length $T = 96$. The best results are in **bold**.

Model	EKPB	iTransformer	TSMixer	Crossformer	FECAM	
Metric	MSE	MAE	MSE	MAE	MSE	MAE
ETTm2	96	0.179 0.260	0.180 0.264	0.182 0.266	0.287 0.366	0.188 0.275
	192	0.244 0.301	0.250 0.309	0.249 0.309	0.414 0.492	0.265 0.336
	336	0.303 0.339	0.311 0.348	0.309 0.347	0.597 0.542	0.318 0.362
	720	0.401 0.395	0.412 0.407	0.416 0.408	1.730 1.042	0.416 0.417
	Avg	0.282 0.324	0.288 0.332	0.289 0.333	0.757 0.610	0.297 0.348
ETTh2	96	0.288 0.338	0.297 0.349	0.319 0.361	0.745 0.584	0.298 0.345
	192	0.374 0.391	0.380 0.400	0.402 0.410	0.877 0.656	0.377 0.397
	336	0.414 0.426	0.428 0.432	0.444 0.446	1.043 0.731	0.425 0.434
	720	0.421 0.440	0.427 0.445	0.441 0.450	1.104 0.763	0.432 0.450
	Avg	0.374 0.399	0.383 0.407	0.401 0.417	0.942 0.684	0.383 0.407
Weather	96	0.166 0.209	0.174 0.214	0.166 0.210	0.158 0.230	0.182 0.242
	192	0.216 0.256	0.221 0.254	0.215 0.256	0.206 0.277	0.223 0.281
	336	0.274 0.296	0.278 0.296	0.287 0.300	0.272 0.335	0.270 0.320
	720	0.351 0.346	0.358 0.349	0.355 0.348	0.398 0.418	0.338 0.374
	Avg	0.252 0.277	0.258 0.279	0.256 0.279	0.259 0.315	0.253 0.304
ECL	96	0.146 0.240	0.148 0.240	0.157 0.260	0.219 0.314	0.178 0.267
	192	0.161 0.254	0.162 0.253	0.173 0.274	0.231 0.322	0.185 0.273
	336	0.178 0.273	0.178 0.269	0.192 0.295	0.246 0.337	0.199 0.290
	720	0.220 0.306	0.225 0.317	0.223 0.318	0.280 0.363	0.235 0.323
	Avg	0.176 0.268	0.178 0.270	0.186 0.287	0.244 0.334	0.199 0.288